Available online at www.sciencedirect.com
ScienceDirect
Advances in Space Research xxx (2009) xxx–xxx
ADVANCES IN SPACE RESEARCH (a COSPAR publication)
www.elsevier.com/locate/asr

Mesospheric OH temperatures: Simultaneous ground-based and SABER OH measurements over Millstone Hill

S.M. Smith [a,*], J. Baumgardner [a], C.J. Mertens [b], J.M. Russell [c], M.G. Mlynczak [b], M. Mendillo [a]

[a] Center for Space Physics, Boston University, Boston, MA 02215, United States
[b] NASA Langley Research Center, Hampton, VA 23681, United States
[c] Center for Atmospheric Sciences, Hampton University, Hampton, VA 23668, United States

Received 18 May 2009; received in revised form 24 September 2009; accepted 25 September 2009

Abstract

We present rotational temperature measurements of the mesospheric OH emission layer using a meridional imaging spectrograph at Millstone Hill (42.6°N, 72.5°W). The system is equipped with a state-of-the-art bare-CCD detector and can yield simultaneous quasi-meridional images of the mesospheric OH and O_2 intensity and temperature fields at 87 and 94 km altitude during the course of each night. A cross-validation study of the rotational OH temperature measurements obtained on 61 nights during the autumnal months of 2005–2007 was undertaken with near-simultaneous kinetic temperature measurements made by the SABER instrument aboard the NASA TIMED satellite during overpasses of Millstone Hill. Excellent agreement was obtained between the two datasets with the small differences being attributable to differences in the spatial and temporal averaging inherent between the two datasets.

Keywords: Mesosphere; Hydroxyl; Nightglow; Temperatures; Spectrograph; Satellite

1. Introduction

The measurement of mesospheric OH rotational temperatures using spectral line ratios is a well-established technique (e.g., Meriwether, 1985; Sivjee, 1992; Greet et al., 1998; Taylor et al., 1999; Pendleton et al., 2000; Bittner et al., 2002; Zhao et al., 2003, 2005; Reisin and Scheer, 2004; Taori et al., 2005; Oberheide et al., 2006). We have developed a meridional spectrographic imaging system at our Millstone Hill, MA field station (42.6°N, 76.5°W) to derive OH temperatures on a nightly basis. The measurements will complement the observations made by the Boston University all-sky imager also located at Millstone Hill. The all-sky imager records nightly gravity wave activity in the three mesospheric emissions; OH, Na, and O(^{1}S) (Baumgardner et al., 1993; 2007; Smith et al., 2000; Smith, 2004; Mendillo et al., 2008).

Overflights of the Millstone Hill site by the NASA Thermosphere, Ionosphere, Mesosphere Energetics and Dynamics (TIMED) satellite mission can provide a useful opportunity to compare and validate the new spectrograph measurements. The Sounding of the Atmosphere using Broadband Emission Radiometry (SABER) instrument aboard the TIMED satellite can provide temperature profiles from 20–140 km altitude and also OH volume emission profiles over the 70–120 km altitude range (Russell et al., 1999; Mertens et al., 2001; Russell and Mlynczak 2003).

Here, we will present the capabilities of the new Millstone Hill spectrograph and compare the new measurements with near-simultaneous temperature and OH emission profile measurements (within 1.5 min) from the SABER instrument during the autumnal months of 2005–2007.

* Corresponding author.
E-mail address: smsm@bu.edu (S.M. Smith).

0273-1177/$36.00 © 2009 COSPAR. Published by Elsevier Ltd. All rights reserved.
doi:10.1016/j.asr.2009.09.022

2. Instrumentation

The Boston University bare-CCD meridional imaging spectrograph (hereafter, MH spectrograph) has been operating at Millstone Hill since March 2005. The instrument utilizes a 1200 lines mm^{-1} grating, yielding a dispersion of 0.01 nm $pixel^{-1}$ and a spectral resolution (FWHM) of 0.25 nm. The spectrograph slit samples approximately 40° of the night sky along the North–South meridian which corresponds to a 60 km × 0.3 km strip of sky at the height of the OH layer (~87 km). Fig. 1 shows the sampled region projected onto an all-sky image of the OH emission obtained with the co-located Boston University all-sky imager. The area sampled for the zenith temperature measurements is shown as the shorter length within 4° of the zenith. The spectrograph operates automatically during the two weeks centered on the New Moon.

The spectral region recorded by the spectrograph is 780–880 nm, a total range of 100 nm (see Fig. 2a). A red blocking filter was placed within the optical path of the spectrograph prior to the dispersion stage to eliminate any possible contamination from other spectral orders. Individual spectra are recorded sequentially with an integration time of 300 s using an Andor 2048 × 2048 13.6 μm-pixel bare-CCD detector cooled to −50 °C. The CCD has a quantum efficiency of ~75% in the near infra-red. The spectra are 2 × 8 binned and digitized to 16-bit resolution prior to readout.

The raw spectra were initially dark-subtracted, flat-fielded and the time exposure times normalized to 1 s. The flat-fielding process characterizes the pixels-to-pixel variations across the chip and involves inserting a diffusing filter into the imaging system and illuminating the system. The resulting flat-field image is then divided into each dark-subtracted spectrum.

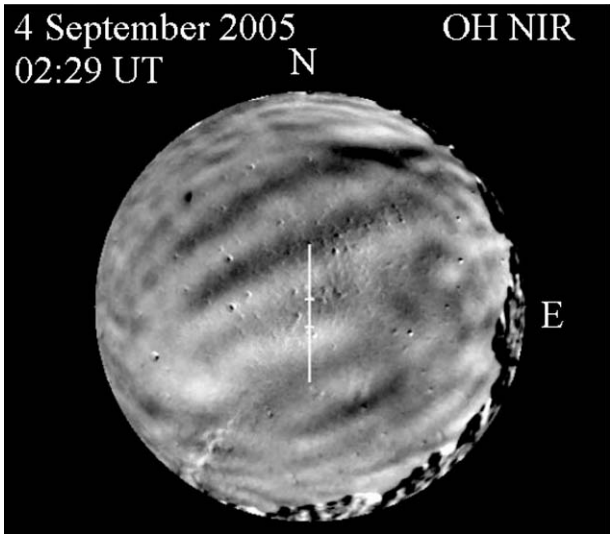

Fig. 1. Time-difference all-sky image (the difference of two consecutive images) in the OH emission, obtained by the Boston University all-sky imager at Millstone Hill. The total area of sky sampled by the spectrograph (40°) is marked by the solid white line. The 8° region used for the zenith temperature determinations is located within the two central marks. A large gravity wave event can be seen propagating towards the NW.

The absolute calibration and stability of the spectrograph is checked annually using the method employed by Baumgardner et al. (2007) in which the spectrograph slit is illuminated by a standard laboratory source. The standard source consists of a low-wattage tungsten standard lamp source which was itself, cross-calibrated originally with a standard C^{14} light source by Galand et al. (2004). The C^{14} source consists of a 2″ diameter phosphor-coated glass disc containing radioactive C^{14} which decays and causes the phosphor to glow. The brightness of C^{14} source has been measured in units of Rayleighs per Ångstrom ($10^6/4\pi$ photons $cm^{-2}\,s^{-1}\,Å^{-1}$) over the visible spectral region.

The effect of vignetting across the visual field of the imager was characterized by illuminating the system with a standard light source from a series of angles distributed between zenith and the horizon. A slice is taken of the resultant overlapping dark-subtracted images and a curve is fitted, yielding a vignetting curve. The curve is then converted into a 2D function, which is symmetrical along the central axis of the spectrum, and then divided into the sky images.

Analysis of the raw spectra for the temperature determinations concentrated on the 830–875 nm spectral region containing the OH(6-2) and O_2(0-1) bands (see Fig. 2b). Wavelength calibration of the spectra was achieved using six identified spectral lines located within the sampled spectral region of interest; 830–875 nm. The spectral dispersion equation for each spectrum was calculated by fitting the line positions at the center of each spectrum (i.e., at zenith) to a 3rd-order polynomial fit through. Spectral line curvature was removed by fitting using a 2nd-order polynomial to three locations along each line.

After photometric and wavelength calibration, the spectra were median-smoothed using a 2 × 2-pixel kernel and sampled over 8°, centered on zenith, which corresponded to a 12-km long strip sampled from an altitude of the OH layer (~87 km) (see Fig. 1). Fig. 3 shows the spectral plot of the sampled area made over the spectral region of interest in Fig. 2b, i.e., 830–875 nm. The OH(6-2) $P_1(2)$ and $P_1(4)$ lines used for calculating the OH rotational temperature are identified.

3. Spectrographic OH rotational temperature determination

The derivation of OH rotational temperatures from spectral line ratios assumes that the OH gas is in local thermodynamic equilibrium (LTE) (Meriwether, 1985; Sivjee, 1992). The radiative lifetime of the OH(v=6) vibrational level is $\sim 6\times10^{-3}$ s (Turnbull and Lowe, 1989). At 87 km altitude, the temperature and pressure is ~200 K and $\sim 2.8 \times 10^{-4}$ kPa, respectively. Hence, the neutral collisional frequency is $\sim 4\times10^4\ s^{-1}$, so the OH($v = 6$) molecules would undergo ~240 collisions prior to radiative

Please cite this article in press as: Smith, S.M., et al. Mesospheric OH temperatures: Simultaneous ground-based and SABER OH measurements over Millstone Hill. J. Adv. Space Res. (2009), doi:10.1016/j.asr.2009.09.022

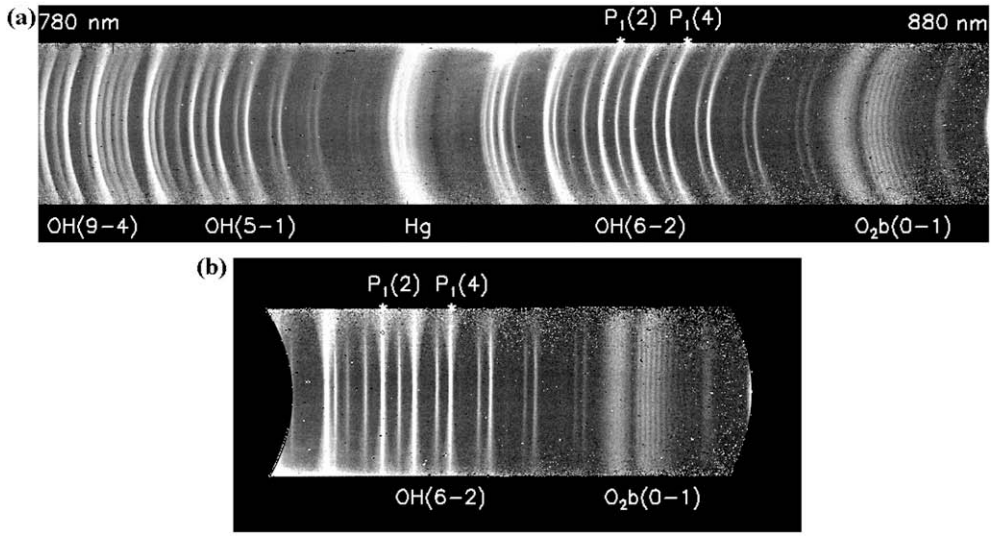

Fig. 2. Examples of the 5-min spectra obtained by the Boston University spectrograph at Millstone Hill. (a) Dark-subtracted, flat-fielded spectrum imaging prior to line straightening. (b) The spectral region of interest (830–875 nm) portion of the spectrum used in OH temperature determination after line straightening.

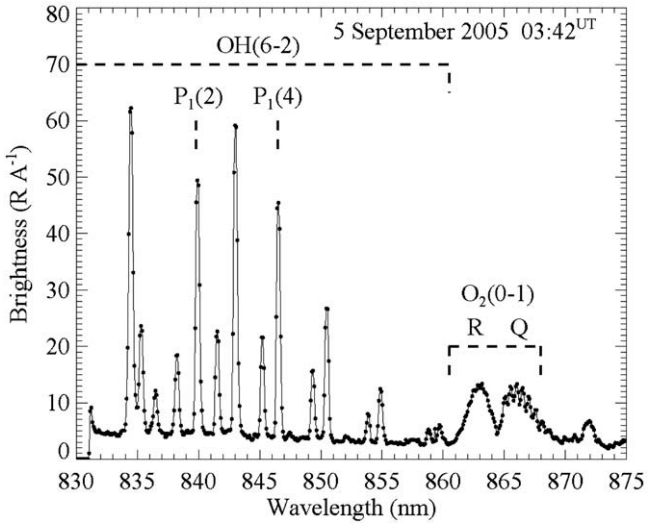

Fig. 3. Zenith slice though a typical individual 5-min spectrum (such as shown in Fig. 2b) obtained by the Boston University spectrograph prior to temperature determination. The Meinel OH(6-2) $P_1(2)$ and $P_1(4)$ lines (840.0 nm and 846.5 nm, respectively) and the O_2 Atmospheric (0-1) band centered near 865.0 nm, are identified.

de-excitation. Since only a few collisions should be required for thermalization of the rotational levels, we would expect, the ro-vibrational emission to reflect a thermal distribution among rotational levels, with the rotational temperature equaling the kinetic temperature, i.e., LTE conditions.

Assuming thermalization of the rotational levels, the OH rotational temperature (T_{rot}) was derived from the Millstone Hill spectrograph measurements by calculating the intensity ratio of the Meinel OH(6-2) $P_1(2)$ and $P_1(4)$ spectral lines (λ-doublets at 840.0 and 846.5 nm, respectively). The intensity of each OH line was determined by integrating over each entire spectral line profile, using a 1.2 nm-wide box-car window, and subtracting a background level determined by a 2nd-order polynomial least-squares fit. The fit utilized 90 points located over the 831–874 nm spectral region located within and near the OH(6-2) and O_2(0-1) bands, and chosen to lie between the bright spectral lines. Similarly, the O_2(0-1) band intensities (originating from ~94 km altitude) were derived by integrating over the 861–870 nm spectral region, after subtracting a baseline level deduced from the 2nd-order polynomial fit.

The Einstein transition probabilities used for the temperature determinations were obtained from Goldman et al. (1998). A correction was made for contamination of the $P_1(2)$ line by the nearby $Q_1(5)$ line. The amount of $Q_1(5)$ contamination is temperature dependent. For example, at 150 K, it amounts to ~0.5%, and at 200 K, ~2.0%, therefore the value was derived iteratively. In addition, a correction for line-blending due to λ-doubling was also made by estimating the contribution due to blending as a function of temperature. The correction amounted to ~2 K at 200 K.

4. Rotational temperature and brightness measurements

The zenith OH temperature measurements obtained by the MH spectrograph typically show marked variability from night to night but all are dominated by large-scale wave-like variations with periods of 3–10 h and amplitudes of 5–10 K. These are probably due to large-scale inertial gravity-waves and tidal oscillations. Smaller-scale perturbations with periods of ~1–2 h are also superimposed upon the larger-scale variations. The typical uncertainties associated with the derived temperature values was 2–3 K. Fig. 4 shows typical examples from the consecutive nights of 3–7

Please cite this article in press as: Smith, S.M., et al. Mesospheric OH temperatures: Simultaneous ground-based and SABER OH measurements over Millstone Hill. J. Adv. Space Res. (2009), doi:10.1016/j.asr.2009.09.022

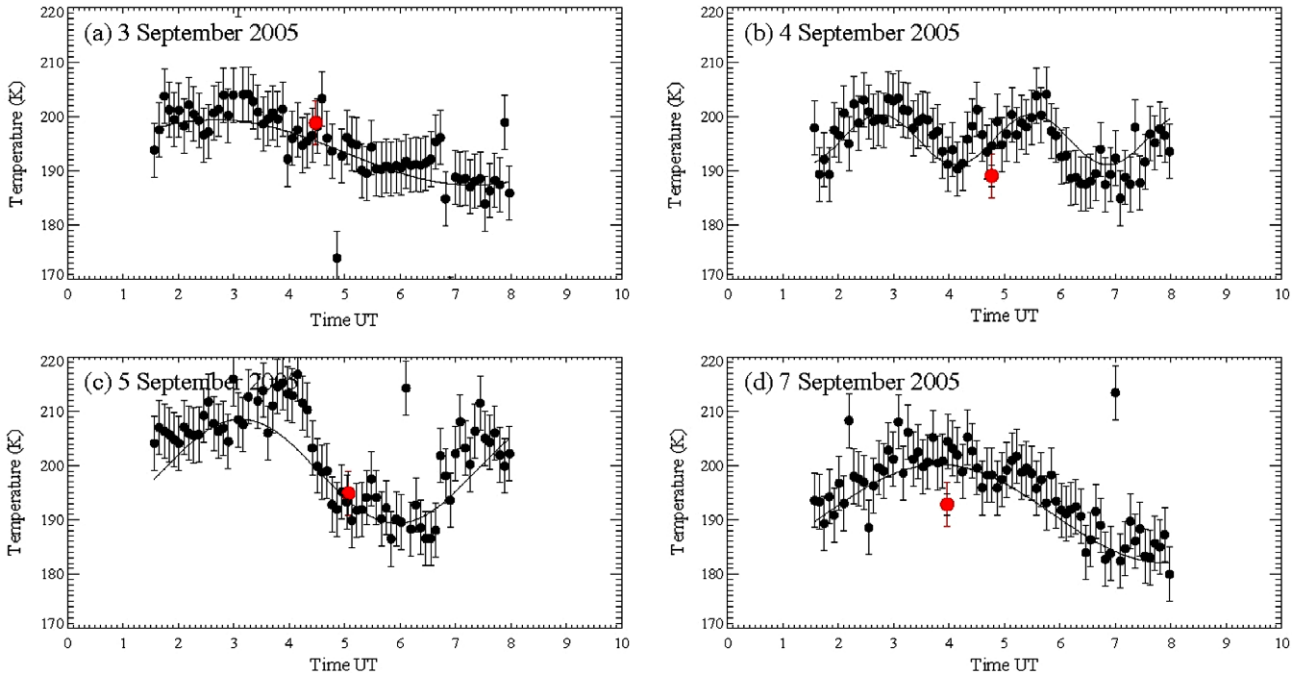

Fig. 4. Zenith OH rotational temperatures obtained with the Boston University spectrograph at Millstone Hill on consecutive nights of 3–7 September 2005 (black circles) with the least-squares fits (solid curves). The red circles are the SABER kinetic temperature measurements made during overpasses of the site.

September 2005. The red circles are the OH emission profile-weighted SABER T_{kin} measurements made during the overpasses of Millstone Hill (described in the next section). The solid curves are the least-squares fits to an arbitrary sinusoid.

Looking at the results obtained from one particular night, 5 September 2005, Fig. 5a shows a large and sudden OH temperature decrease of almost 25 K that occurred near 04:00 UT. Concurrent all-sky imager data (not shown) indicated the passage of a large frontal gravity wave occurred at that time. Fig. 5b shows the corresponding zenith brightness variations of the individual $P_1(2)$ and $P_1(4)$ lines of the OH(6-2) band and also the $O_2(0\text{-}1)$ band during the course of the night. The OH temperature variations in Fig. 5a match closely the $O_2(0\text{-}1)$ band brightness variations in Fig. 5b, a result of the different sampling altitudes of the airglow brightness and temperature fields inherent in ground-based measurements which utilize integrated line of sight sampling (Swenson and Gardner, 1998).

5. Quasi-Imaging of the temperature and brightness fields

The spectrograph slit is projected onto the sky along the N–S meridian. Therefore the spectra can yield spatial information about each emission along the slit direction. By sampling spectral regions of interest, in this case two OH(6-2) band lines and the $O_2(0\text{-}1)$ band, one can construct quasi-images of the time histories of the brightness or temperature variations from several emissions simultaneously over the course of the night. Specifically, for a given spectrum, an individual line is sampled along its length. Each line (usually 4–5 pixels wide) is then averaged down into a single 1D array which then becomes a column in a 2D array. A schematic diagram of this procedure is presented in Fig. 6. The process is repeated for subsequent spectra and a 2D "image" consisting of one particular spectral line is built up over the course of the night. The spatial direction is in the vertical direction, along the length of the spectral line, and the time dimension is in the horizontal direction.

Fig. 7 shows this approach in practice using the measurements from the night of 5 September 2005. In each panel, as described above, time increases horizontally along the x-axis and the spatial dimension (N–S) is in the vertical direction. Each spectral line has been averaged down into a single vertical pixel column. Millstone Hill is located along the middle of each plot, level with the "Z" symbol. In each panel, the northward direction is upwards and southward direction downwards and, as described earlier, the vertical spatial extent of each panel is 60 km at 90 km. Fig. 7a and b shows "images" of the $P_1(2)$ and $P_1(4)$ line brightness during the night, respectively, and the $O_2(0\text{-}1)$ band brightness is shown in Fig. 7c. Fig. 6d shows the resulting OH rotational temperature variation, essentially the ratio of Fig. 7a and 7b. The temperature "image" shows clear meridional gradients in the OH temperature field as well as temporal temperature variations. The technique provides a means of yielding spatial temperature information with little or no contamination from scattered light compared to traditional imaging methods using a series

Please cite this article in press as: Smith, S.M., et al. Mesospheric OH temperatures: Simultaneous ground-based and SABER OH measurements over Millstone Hill. J. Adv. Space Res. (2009), doi:10.1016/j.asr.2009.09.022

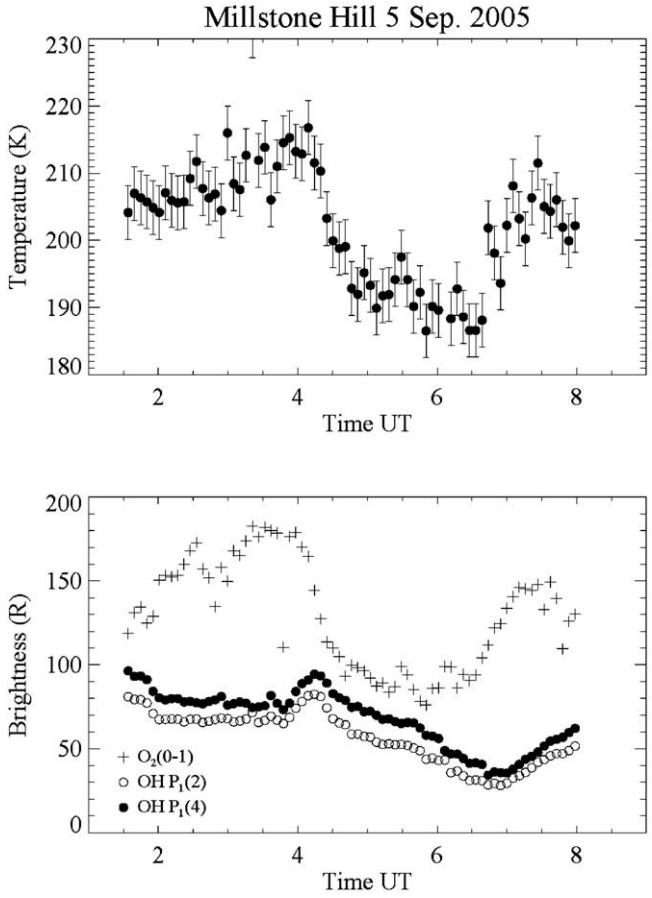

Fig. 5. Zenith measurements of (a) OH rotational temperatures and (b) $P_1(2)$ and $P_1(4)$ OH(6-2) line and $O_2(0\text{-}1)$ band brightness obtained by the Millstone Hill spectrograph on 5 September 2005.

narrow-band filters. Furthermore, unlike multi-spectral all-sky or wide-field imaging, where several emissions are recorded sequentially with a single system, the spectrograph records all of the measured parameters simultaneously.

6. Millstone Hill spectrograph/SABER temperature comparisons

The SABER instrument is one of four experiments aboard the NASA TIMED satellite. The instrument obtains Earth limb scan measurements (~20–450 km tangent-height range) of the CO_2 emission at 15 μm and 4.3 μm, from which kinetic temperature (T_{kin}) altitude profiles and, during the daytime, CO_2 mixing ratio profiles are simultaneously retrieved, respectively, from a non-LTE retrieval algorithm (Mertens et al., 2001). Each scan takes ~53 s (Russell et al., 1999; Russell and Mlynczak, 2003). At night, only T_{kin} is retrieved and the CO_2 profiles are obtained from TIME-GCM climatology (Mertens et al., 2004). The estimated uncertainty in the SABER temperature profiles in the altitude range of 80–100 km is ~4 K (Mertens et al., 2001). The SABER instrument also measures the mesospheric hydroxyl (OH) volume emission limb profiles at 1.6 μm (OH-B channel) and 2.0 μm (OH-A channel).

The 67 temperature comparisons were made during 61 nights during the months of August–November in 2005–2007 using the SABER OH-B channel, which is centered at 1640 nm with a bandwidth (FWHM) of 8.0 nm. The channel contains the Meinel OH(4-2) and OH(5-3) bands at 1.55–1.63 μm and 1.63–1.75 μm, respectively, and a small portion of the OH(6-4) band at 1.72–1.75 μm. The SABER temperature and OH data used in the comparison study was version 1.07 obtained from http://saber.gats-inc.com.

During the 61 nights, there were a total of 67 individual overpasses, all of which occurred within 500 km of Millstone Hill. The nightly mean height of maximum OH emission measured by SABER during each overpass was 87.1 km ($\sigma = 2.2$ km), with a mean FWHM emission layer width of 8.1 km ($\sigma = 1.8$ km). For each comparison, the temperature measurement closest in time to each TIMED overpass was used. In 93% of the cases (62 overpasses) of cases the time difference between the two measurements was less than 93 s. For the other 7% (5 overpasses) the time differences ranged from 0.2 to 1.2 h. In those cases, the overpasses occurred prior to or after time of the ground-based measurements.

Prior to the comparison, the SABER T_{kin} profiles were weighted vertically by the OH-B volume emission profiles (at ~1.6 μm) in order to approximate the vertically integrating sampling regime that was utilized by the ground-based spectrograph. The observed uncertainty in the emission profile measurements was 10% (Russell et al., 1999; Russell and Mlynczak, 2003).

Fig. 8 is a correlation plot showing the two datasets. The slope of best fit (shown) is 0.91 ± 0.15 with a correlation coefficient of $r = 0.72$, which was statistically significant to >99.9% confident level. There is clearly very good agreement between the two data sets, especially considering the differences in spatial and temporal averaging inherent in the two measurements. The SABER instrument, being a limb-scanning instrument, can sample small vertical scale-sizes (~2–3 km) but only large horizontal scale-sizes (~400 km). Ground-based instruments, such as the Millstone spectrograph, other the hand can sample small horizontal scale-sizes (~1–2 km) and short-period wave variations (<1 h) and vertical scale-sizes larger than ~10–15 km, due to their integrating technique. Furthermore, the spectrograph integrates for 300 s compared to 53 s for SABER to perform a limb scan.

The mean temperature difference between the two datasets (SABER minus MH spectrograph) was −1.7 K ($\sigma = 9.5$ K), i.e., the SABER temperatures were colder. Several correlative studies of SABER and ground-based measurements have consistently yielded similar mean differences. For example, Oberheide et al. (2006) reported that SABER temperatures during the three-year period of 2003–2005 were systematically 7.5 ± 7.5 K lower than the corresponding OH(3-1) ground temperatures, independent of season or year. Similarly, Lopez-Gonzalez

Please cite this article in press as: Smith, S.M., et al. Mesospheric OH temperatures: Simultaneous ground-based and SABER OH measurements over Millstone Hill. J. Adv. Space Res. (2009), doi:10.1016/j.asr.2009.09.022

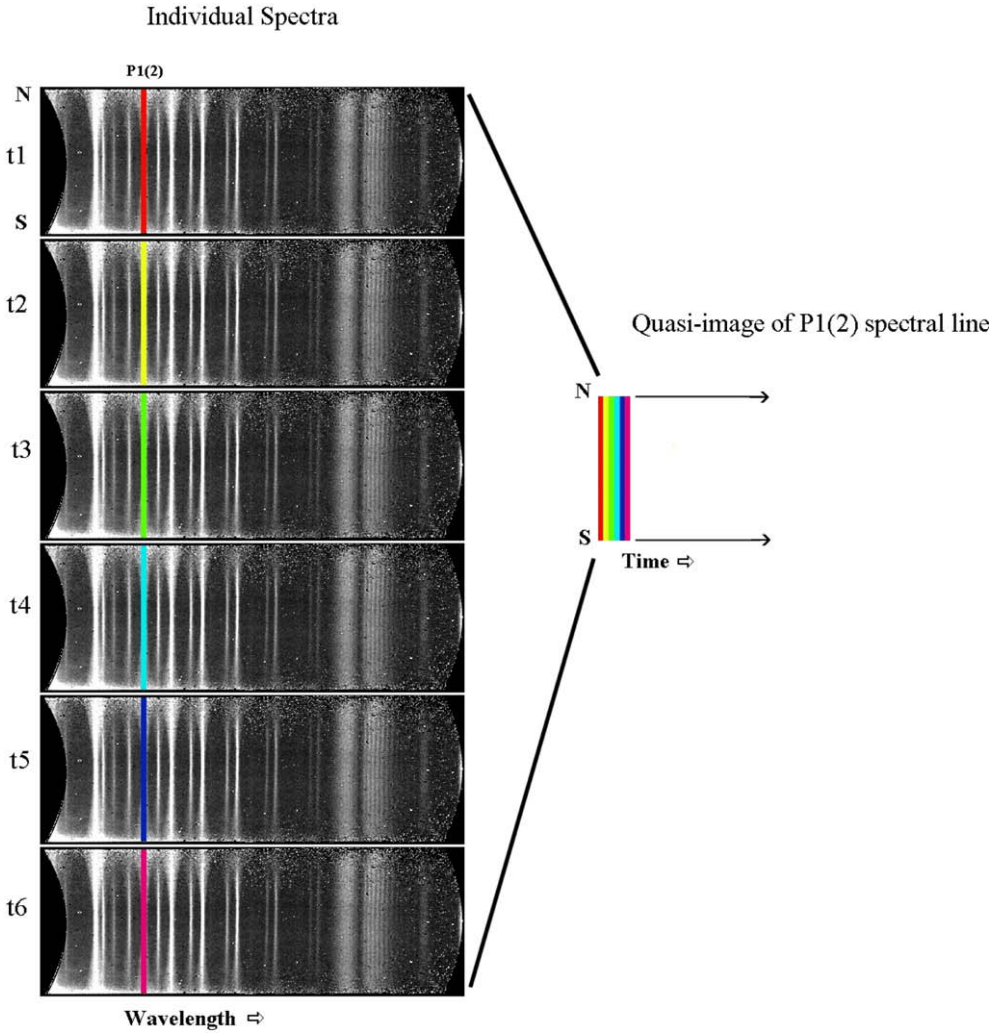

Fig. 6. Schematic diagram of the procedure of deriving a quasi-image of a spectral line from the a series of individual consecutive spectral at times t1, t2, t3, ..., t6. Here, the $P_1(2)$ OH(6-2) line (multi-colored) is selected from each spectrum on the left and combined to build up in image on the right.

et al. (2007) found differences of 5.7 ± 7.0 K for OH(6-2) temperatures. Both comparsions used version 1.06 SABER temperature data. A large comparative study using version 1.07 SABER data and optical airglow and lidar measurements (Remsberg et al., 2008) found that the SABER temperatures to be 2–3 K colder compared to the ground-based measurements. For example, during 2003, the mean difference with ground-based OH(6-2) temperatures was 5.8 ± 8.9 K, the SABER temperatures were colder by that amount.

The excellent agreement between the T_{rot} and T_{kin} measurements also suggests that the rotational levels were thermalized totally during the observations. Hence, the differences observed between the two datasets can be explained to be the result of sampling differences between the two observing techniques, i.e., different volumes and sampling times, even though they sample similar regions simultaneously.

7. Summary

Rotational temperatures have been determined from imaging spectrograph measurements of the night-time mesospheric OH nightglow over Millstone Hill. The temperatures were derived from line strength ratio measurements of the $P_1(2)$ and $P_1(4)$ lines of the OH(6-2) Meinel band near 840 nm. We also presented a method of imaging the OH and O_2 airglow brightness and temperature fields within 40° of zenith using the MH spectrograph data. The method provides a way of obtaining truly simultaneous intensity and temperature measurements from several different emissions and altitude regions.

Sixty-seven individual MH spectrograph temperature measurements obtained on 61 nights during the autumnal months of 2005–2007 were compared to kinetic temperatures at the same height region (~87 km) obtained from the SABER instrument aboard the NASA TIMED satellite

Please cite this article in press as: Smith, S.M., et al. Mesospheric OH temperatures: Simultaneous ground-based and SABER OH measurements over Millstone Hill. J. Adv. Space Res. (2009), doi:10.1016/j.asr.2009.09.022

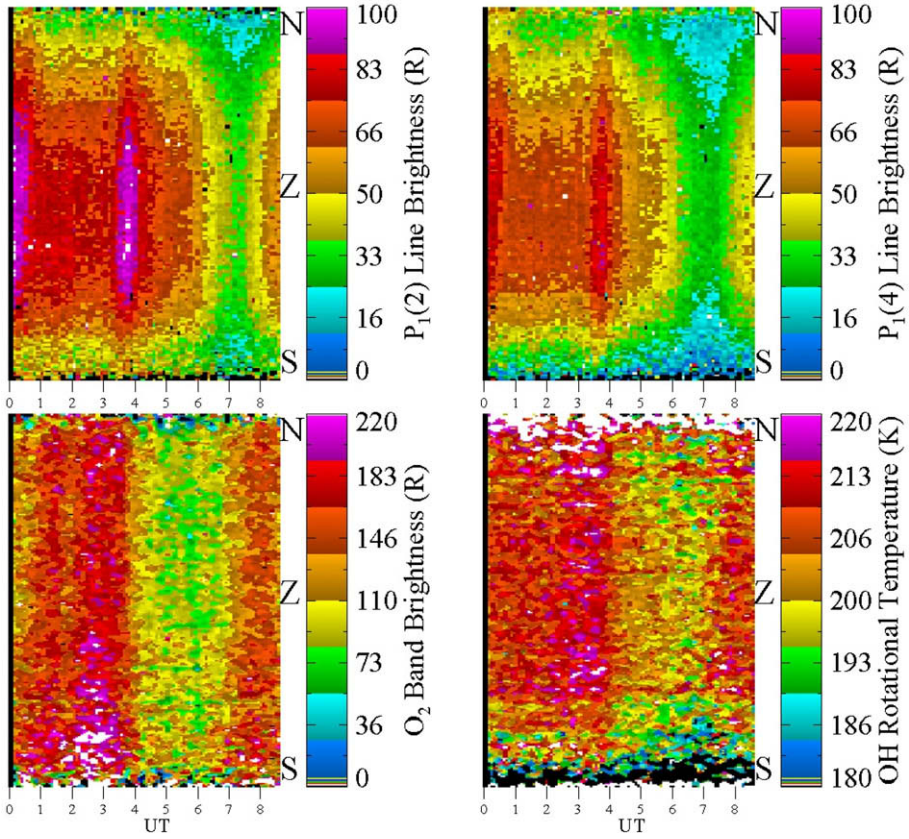

Fig. 7. Quasi-images of derived of (a) $P_1(2)$ OH(6-2) line brightness. (b) $P_1(4)$ OH(6-2) line brightness. (c) O_2(0-1) band brightness. (d) OH rotational temperature obtained by the Millstone Hill spectrograph on 5 September 2005.

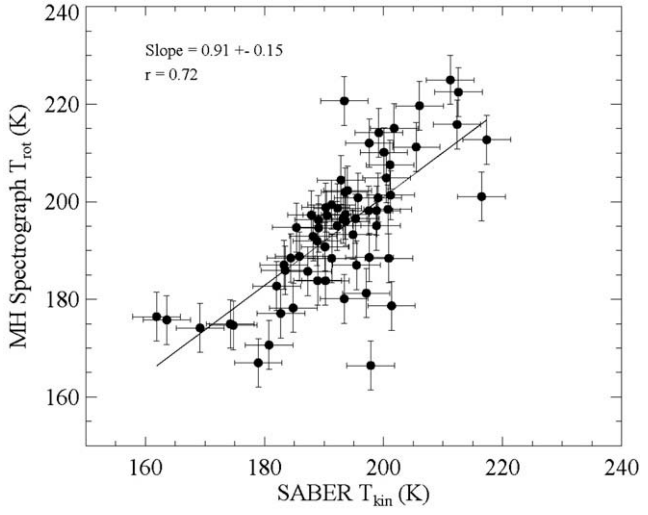

Fig. 8. Correlation plot of the 67 simultaneous SABER and spectrograph temperatures from August–November 2005–2007. The correlation coefficient is 0.72, significant to the 99.9% level, and the line of best fit (solid line) is 0.91 ± 0.15. The mean temperature difference between the two datasets 23w (SABER minus Millstone) was -1.7 K ($\sigma = 9.5$ K).

during overpasses of the Millstone Hill site. Excellent agreement between the two datasets was found ($r = 0.72$) with the mean temperature difference being -1.7 K ($\sigma = 9.5$ K); the SABER temperatures being slightly colder, which is a similar finding to recent studies.

Acknowledgments

This study was supported by the NSF CEDAR program under Grant ATM-0123064 and the NSF Aeronomy Program under Grant ATM-0322875. S.M.S., J.B. and M.M. would like to thank the director and staff at the MIT Haystack Observatory for their continued support for our observation program. M.G.M. acknowledges the support of the SABER project from the NASA Science Mission Directorate and the NASA Langley Science Directorate.

References

Baumgardner, J., Flynn, B., Mendillo, M. Monochromatic imaging instrumentation for applications in aeronomy of the Earth and planets. Opt. Eng. 32 (12), 3028–3032, 1993.

Baumgardner, J., Wroten, J., Semeter, J., Kozyra, J., Buonsanto, M., Erickson, P., Mendillo, M. A very bright SAR arc: implications for extreme magnetosphere-ionosphere coupling. Ann. Geophys. 25 (12), 2593–2608, 2007.

Bittner, M., Offermann, D., Graef, H.-H., Donner, M., Hamilton, K. An 18-year time series of OH rotational temperatures and middle atmosphere decadal oscillations. J. Atmos. Solar Terr. Phys. 64, 1147–1166, 2002.

Galand, M., Baumgardner, J., Pallamraju, D., Chakrabarti, S., Løvhaug, U.P., Lummerzheim, D., Lanchester, B.S., Rees, M.H. Spectral imaging of proton aurora and twilight at Tromsø, Norway. J. Geophys. Res. 109, A07305, doi:10.1029/2003JA010033, 2004.

Goldman, A., Schoenfeld, W.G., Goorvitch, D., Chackerian, C., Dothe, H., Melen, F., Abrams, M.C., Selby, J.E.A. Updated line parameters for OH X^2 II–X^2 II(v″,v′) transitions. J. Quant. Spectrosc. Radiat. Transfer 59 (3–5), 453–469, 1998.

Greet, P.A., French, W.J.R., Burns, G.B., Williams, P.F.B., Lowe, R.P., Finlayson, K. OH(6-2) spectra and rotational temperature measurements at Davis, Antartica. Ann. Geophys. 16, 77–89, 1998.

Lopez-Gonzalez, M.J., Rodriguez, E., Lopez-Puertas, M., Garcia-Comas, M., Shepherd, M.G., Shepherd, G.G., Sargoytchev, S., Aushec, M., Smith, S.M., Mlynczak, M.G., Russell, J.M., Brown, S., Cho, Y.M., Wein, R.H. Ground-based mesospheric temperatures at mid-latitude derived from O_2 and OH airglow SATI data: comparison with SABER measurements. J. Atmos. Solar Terr. Phys. 69, 2379–2390, 2007.

Mendillo, M., Smith, S.M., Coster, A., Erickson, P., Baumgardner, J., Martinis, C. Man-Made Space Weather, Space Weather 6, S09001, doi:10.1029/2008SW000406, 2008.

Meriwether, J.W. Ground-based measurements of mesosphere temperatures by optical means. In: Vincent, R.A. (Ed.) Middle Atmosphere Program Handbook for MAP, vol. 13, pp. 19–40, 1985.

Mertens, C.J., Mlynczak, M.G., Lopez-Puertas, M., Wintersteiner, P.P., Picard, R.H., Winick, J.R., Gordley, L.L., Russell III, J.M. Retrieval of mesospheric and lower thermospheric kinetic temperature from measurements of CO_2 15-μm Earth limb emission under non-LTE conditions. Geophys. Res. Lett. 28, 1391–1394, 2001.

Mertens, C.J., Schmidlin, F.J., Goldberg, R.A., Remsberg, E.E., Pesnell, W.D., Russell III, J.M., Mlynczak, M.G., Lopez-Puertas, M., Wintersteiner, P.P., Picard, R.H., Winick, J.R., Gordley, L.L. SABER observations of mesospheric temperatures and comparisons with falling sphere measurements taken during the 2002 summer MaCWAVE campaign. Geophys. Res. Lett. 31, l03105, doi:10.1029/2003gl018605, 2004, 2004.

Oberheide, J., Offermann, D., Russell III, J.M., Mlynczak, M.G. Intercomparison of kinetic temperature from 15 μm CO_2 limb emissions and OH^*(3,1) rotational temperature in nearly coincident air masses: SABER, GRIPS. Geophys. Res. Lett. 2006GL026439, 2006.

Pendleton, W.R., Taylor, M.J., Gardner, L.C. Terdiurnal oscillations in OH Meinel rotational temperatures for fall conditions at northern mid-latitude sites. Geophys. Res. Lett. 27 (12), 1799–1802, 2000.

Reisin, E.R., Scheer, J. Gravity wave activity in the mesopause region from airglow measurements at El Leoncito. J. Atmos. Solar-Terrest. Phys. 66 (6–9), 655–661, doi:10.1016/j.jastp.2004.01.017, 2004.

Remsberg, E.E., Marshall, B.T., Garcia-Comas, M., Krueger, D., Lingenfelser, G.S., Martin-Torres, J., Mlynczak, M.G., Russell III, J.M., Smith, A.K., Zhao, Y., Brown, C., Gordley, L.L., Lopez-Gonzalez, M.J., Lopez-Puertas, M., She, C.-Y., Taylor, M.J., Thompson, R.E. Assessment of the quality of the Version 1. 07 temperature-versus-pressure profiles of the middle atmosphere from TIMED/SABER. J. Geophys. Res. 113, D17101, doi:10.1029/2008JD010013, 2008.

Russell, J.M. III, Mlynczak, M.G., Gordley, L.L., Tansock, J., Esplin, R. An overview of the SABER experiment and preliminary calibration results. In: Proceedings of the SPIE, 44th Annual Meeting, Denver, Colorado, vol. 3756, July 18–23, pp. 277–288, 1999.

Russell, J.M., Mlynczak, M.G. SABER Science, Measurement Approach, and Data Product Overview. Available at http://saber.larc.nasa.gov, 2003.

Sivjee, G.G. Airglow hydroxyl emissions. Planet. Space Sci. 40, 235–242, 1992.

Smith, S.M., Mendillo, M., Baumgardner, J., Clark, R.R. Mesospheric gravity wave imaging at a sub-auroral site: first results from Millstone Hill. J. Geophys. Res. 105, 27119–27130, 2000.

Smith, S.M. A survey of all-sky imaging measurements of bore- and "wall"-like disturbances in mesospheric nightglow. American Geophysical Union, Spring Meeting 2004, abstract #SA21A-02, 2004.

Swenson, G.R., Gardner, C.S. Analytical models for the responses of the mesospheric OH^* and Na layers to atmospheric gravity waves. J. Geophys. Res. 103 (D6), 6271–6294, 1998.

Taori, A., Taylor, M.J., Franke, S. Terdiurnal wave signatures in the upper mesosphere temperature and their association with the wind fields at low latitudes (20°N). J. Geophys. Res. 110, D09S06, doi:10.1029/2004JD004564, 2005, 2005.

Taylor, M.J., Pendleton, W.R., Gardner, C.S., States, R.J. Comparison of terdiurnal tidal oscillations in mesospheric OH rotational temperature measurements at mid-latitudes for fall/spring conditions. Earth Planets Space 51, 877–885, 1999.

Turnbull, D.N., Lowe, R.P. New hydroxyl transition probabilities and their importance in airglow studies. Planet. Space Sci. 37 (6), 723–738, 1989.

Zhao, Y., Taylor, M.J., Mertens, C.J., Russell, J.M., J.M. Comparison of TIMED/SABER non-LTE temperature retrievals with ground based mesospheric temperature mapper measurements. EOS Trans. AGU, 84(46), Fall Meet. Suppl., Abstract SA41B-0444, 2003.

Zhao, Y., Taylor, M.J., Chu, X. Comparison of simultaneous Na lidar and mesospheric nightglow temperature measurement and the effects of tides on the emission layer heights. J. Geophys. Res. 110, D09S07, doi:10.1029/2004JD005115, 2005, 2005.

Please cite this article in press as: Smith, S.M., et al. Mesospheric OH temperatures: Simultaneous ground-based and SABER OH measurements over Millstone Hill. J. Adv. Space Res. (2009), doi:10.1016/j.asr.2009.09.022